Emergent Biological Endurance Depends on Extracellular Matrix Composition of Three-Dimensionally Printed Escherichia coli Biofilms

Balasubramanian, Srikkanth; Yu, Kui; Cardenas, Diana Vasquez; Aubin-Tam, Marie Eve; Meyer, Anne S.

Important note
To cite this publication, please use the final published version (if applicable).
Please check the document version above.

Emergent Biological Endurance Depends on Extracellular Matrix Composition of Three-Dimensionally Printed *Escherichia coli* Biofilms

Srikkanth Balasubramanian, Kui Yu, Diana Vasquez Cardenas, Marie-Eve Aubin-Tam,* and Anne S. Meyer*

Read Online

ACCESS | 📊 Metrics & More | 📖 Article Recommendations | 🆂🅸 Supporting Information

ABSTRACT: Biofilms are three-dimensional (3D) bacterial communities that exhibit a highly self-organized nature in terms of their composition and complex architecture. Bacteria in biofilms display emergent biological properties, such as resistance to antimicrobials and disinfectants that the individual planktonic cells lack. Bacterial biofilms possess specialized architectural features including unique extracellular matrix compositions and a distinct spatially patterned arrangement of cells and matrix components within the biofilm. It is unclear which of these architectural elements of bacterial biofilms lead to the development of their emergent biological properties. Here, we report a 3D printing-based technique for studying the emergent resistance behaviors of *Escherichia coli* biofilms as a function of their architecture. Cellulose and curli are the major extracellular-matrix components in *E. coli* biofilms. We show that 3D-printed biofilms expressing either curli alone or both curli and cellulose in their extracellular matrices show higher resistance to exposure against disinfectants than 3D prints expressing either cellulose alone or no biofilm-matrix components. The 3D-printed biofilms expressing cellulose and/or curli also show thicker anaerobic zones than nonbiofilm-forming *E. coli* 3D prints. Thus, the matrix composition plays a crucial role in the emergent spatial patterning and biological endurance of 3D-printed biofilms. In contrast, initial spatial distribution of bacterial density or curli-producing cells does not have an effect on biofilm resistance phenotypes. Further, these 3D-printed biofilms could be reversibly attached to different surfaces (bacterial cellulose, glass, and polystyrene) and display resistance to physical distortions by retaining their shape and structure. This physical robustness highlights their potential in applications including bioremediation, protective coatings against pathogens on medical devices, or wastewater treatment, among many others. This new understanding of the emergent behavior of bacterial biofilms could aid in the development of novel engineered living materials using synthetic biology and materials science approaches.

KEYWORDS: 3D bioprinting, synthetic biology, biofilms, cellulose, curli fibers, disinfectant resistance
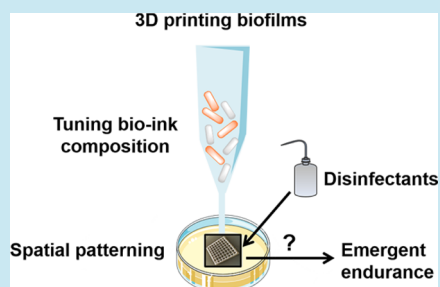
INTRODUCTION

Bacterial biofilms are three-dimensional (3D) assemblages of bacteria in a self-generated matrix (composed of proteins, polysaccharides, lipids, and extracellular DNA) that strongly attach to biotic or abiotic surfaces.[1−4] Biofilms are widely present in natural, medical, and industrial settings.[5,6] Depending on the context, biofilms can be regarded as harmful (e.g., causing device-related infections, sepsis, food-borne infections, etc.) or beneficial (e.g., in degradation of toxic chemicals, bioremediation, bioleaching, sustainable material production, etc.).[7] Bacteria in biofilms substantially differ from their free-living or planktonic counterparts in terms of their resilience and adaptability to extreme conditions, including the presence of antimicrobials, solvents, detergents, high temperature, and so forth.[8−11] Bacterial cells in a biofilm exhibit emergent biological properties (e.g., resistance to antimicrobials/disinfectants) and mechanical properties (viscoelastic nature) that individual planktonic cells do not possess. The resilient nature of cells in a biofilm is thought to arise as a consequence of local physical interactions between different or individual extracellular-matrix components within a biofilm.[12] The emergent endurance of biofilms is frequently associated with factors including the structure, composition, architecture, spatial organization, or mechanical properties (including cohesiveness, viscoelastic nature, resistance to hydrodynamic shear, and stiffness) of constituent biofilm molecules.[13−15] Recently, there has been a growing interest in investigating these emergent properties of bacteria in biofilms.[13,16] While the contribution of individual extracellular-matrix components in the biofilm to the emergent

mechanical properties has been studied,[13] their contribution to the emergent biological endurance remains poorly understood.

The emergent resistance properties of biofilms must be due to the unique features of the biofilms that planktonic cells do not possess, such as the presence of extracellular-matrix components and/or their spatial structuring. The spatial structuring of natural biofilms is governed by parameters including local bacterial density, biofilm matrix composition and density, and so forth. These crucial variables have been hypothesized[10] to have dynamic consequences on the distribution of molecular oxygen and the emergent biological and mechanical endurance of biofilms.[10,12,17] However, it has been impossible to study and control these variables individually, such that the ultimate design principles of biofilms remain unknown. Tuning these variables and studying their emergent consequences can generate useful information about the structure−function relationships of bacterial biofilms over time, leading to better understanding of the underlying biology.[10] Further, since the majority of human infections are caused by biofilm-forming bacteria,[18] elucidating the causes of emergent biofilm resistance behavior can facilitate better design of new antibiofilm strategies. Beyond the fundamental or medical nature of such studies, these emergent properties of biofilms could serve as new platforms for construction of robust next-generation smart materials using synthetic biology and materials science approaches.[17,19,20] However, the challenge here lies in achieving top-down spatial patterning of the biofilm components in order to study their effect on the emergent biological properties.

3D printing is a robust technology that can be used to tackle this challenge. With the development of 3D bioprinting, it is now possible to intentionally alter the spatial patterning of individual extracellular-matrix components and probe their contributions to the emergent resistance phenotypes of biofilms. 3D printing has been increasingly used for the fabrication of living functional materials from nano- to macroscales through printing algae, bacteria, fungi, yeast, plant, and animal cells.[21−31] 3D printing allows for the spatial patterning of constituents mimicking the complex 3D microenvironments and time-evolving nature of living systems.[32−34] The spatial heterogeneity and mechanical robustness of natural biofilms can be simulated with a high degree of control over freedom of shape, design, and resolution provided by 3D printing. 3D-printed biofilm models can potentially better mimic the 3D organization of natural biofilms than conventionally studied biofilms (grown in liquid media or agar) in the laboratory and can be employed for studying fundamental topics including emergent biological endurance to antimicrobials.[35] We have previously shown that biofilms of the Gram-negative bacterium *Escherichia coli* can be effectively 3D-printed into desirable patterns at the sub-millimeter scale resolution using a do-it-yourself home-built 3D printer.[36,37] The extracellular matrix of *E. coli* biofilms is primarily composed of curli fibers, a proteinaceous component, and/or cellulose, a polysaccharide component.[5,13,14,38,39] This nanocomposite matrix has been suggested to confer biological and mechanical endurance to the *E. coli* cells.[40] Thus, tuning the matrix composition and the design principles of *E. coli* biofilms with 3D printing is a powerful approach to analyze the effect of biofilm composition and architecture on their emergent endurance.

Herein, we report a simple approach for spatial patterning of different *E. coli* strains and studying the emergent biological endurance of their biofilms using 3D printing technology (Figure 1). We employed a customized do-it-yourself 3D printer[23,36] for arbitrary patterning of biofilm-forming *E. coli*
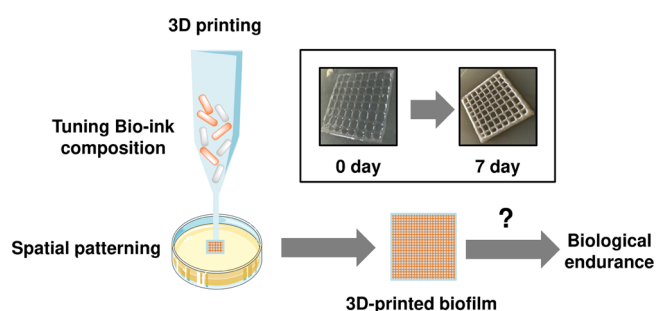

Figure 1. 3D printing of bacterial biofilms for studying their emergent biological endurance. Altering the bioink composition (by mixing one or two different types of biofilm-forming *E. coli* together with sodium alginate) and printing them into spatially defined patterns result in the formation of 3D-printed biofilms over time. These biofilms closely mimic the spatial heterogeneity found in natural biofilms and could be readily used for understanding the emergent biological endurance to disinfectants. This illustration was created with images from https://smart.servier.com/.

onto agar substrates. Different strains of *E. coli* expressing cellulose+/curli+, cellulose−/curli+, and cellulose−/curli− in their biofilm matrix were 3D-printed as four-layered constructs and tested for their emergent biological endurance to disinfectants. We demonstrate that the bacterial biofilms can be effectively 3D-printed into different shapes, and the 3D-printed biofilms display emergent resistance to commonly used laboratory disinfectants such as ethanol and Virkon S. Particularly, we show that tuning the biofilm matrix composition and design principles, such as alteration of bacterial, curli, or cellulose density, through the design of the bioink and 3D printing process has a major influence on the development of resistance toward these disinfectants. For strains expressing curli and/or cellulose, the diffusion of molecular oxygen into the 3D-printed biofilms is limited, and anaerobic zones exist in the lower layers of the biofilm. Further, these 3D-printed biofilms exhibit striking resistance to physical distortions and stably retain their original shape. The 3D prints can be reversibly attached and detached to different surfaces such as bacterial cellulose, glass, and polystyrene, demonstrating their utility in beneficial applications including probiotic biofilm coatings on medical devices, bioremediation, and wastewater treatment plants, among many others.

■ RESULTS AND DISCUSSION

3D Printing *E. coli* Biofilms with Different Extracellular Matrix Compositions. Since the matrix of *E. coli* biofilms is predominantly composed of cellulose and curli,[5,40] we employed three different strains of *E. coli* expressing curli and/or cellulose: *E. coli* Nissle wildtype (cellulose+/curli+); *E. coli* MG1655 Δ*csgA* carrying a plasmid for expression of constitutive green fluorescent protein (GFP) and rhamnose-inducible CsgA (cellulose−/curli+); and *E. coli* MG1655 Δ*csgA* (cellulose−/curli−).for studying the contribution of biofilm-matrix polymers and their spatial distribution to emergent biological endurance. We utilize the inducible curli by preparing media and bioink without an inducer and then depositing or printing the bacteria onto surfaces containing the inducer. In this way, biofilm production only begins after deposition, resulting in reproducible curli production for both biofilms and biofilm prints. *E. coli* Nissle (cellulose+/curli+) is a natural biofilm-forming strain that has a different strain background from the two *E. coli* MG1655 strains (cellulose−/curli+ and cellulose−/curli−). As such, the
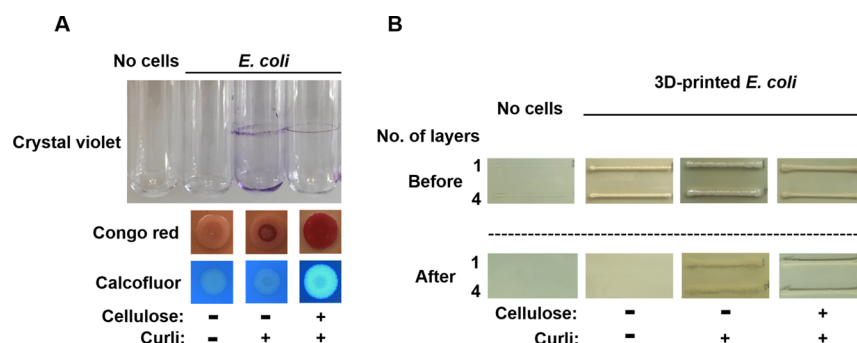
Figure 2. Biofilm formation by *E. coli* strains in this study. (A) Crystal violet (top), Congo red (middle), and calcofluor assays (bottom) for visualization of total biofilm and to identify the biofilm-matrix components. The crystal violet assay detects the total biofilm formation in liquid culture, whereas the Congo red assay detects the presence of cellulose and/or curli, and the calcofluor assay detects the presence of cellulose in colony biofilms (hydrogel culture) and (B) resistance of 3D-printed biofilms (one- or four-layered prints) to citrate treatment. Images on the top depict 3D-printed biofilms before citrate treatment, and the images on the bottom depict 3D-printed biofilms after citrate treatment. All biofilm samples were grown at room temperature for 7 days before these experiments were carried out.

Nissle strain is included in these studies as a positive control representing a natural 3D-printed biofilm to compare to our engineered 3D-printed biofilms. In *E. coli*, cellulose and curli are better expressed under lower temperature conditions (<30 °C) due to the transcriptional regulator CsgD that upregulates the expression of both curli and cellulose.[5] Therefore, all biofilm formation assays were carried out under room-temperature conditions.

Biofilm formation by our experimental strains and the presence of cellulose and/or curli were evaluated by three different staining assays: crystal violet, Congo red, and calcofluor (Figure 2). For the first assay, the ability of the strains to form biofilms in liquid culture was evaluated by a crystal violet biofilm assay performed in glass test tubes (Figure 2A). The formation of biofilms at air−liquid boundaries is characteristic of *E. coli* biofilms.[12] *E. coli* strains expressing no cellulose but only curli (cellulose−/curli+) or both cellulose and curli (cellulose+/curli+) were able to form biofilms, as visualized from a crystal violet-stained ring formed at the air−liquid interface in the culture tube. In contrast, no crystal violet staining was seen in *E. coli* strains that expressed neither cellulose nor curli (cellulose−/curli−) or the no-bacteria samples.

E. coli are also known to form biofilms on gel−air boundaries when grown as colonies on agar plates.[13] Therefore, in the second assay, the presence of curli and/or cellulose in colony biofilms was visualized by the binding of the diazo dye Congo red to these biofilms.[14,41] Strains expressing cellulose and/or curli (cellulose+/curli+ and cellulose−/curli+) appeared red in color due to the binding of Congo red to cellulose and/or curli fibers, confirming the presence of curli and/or cellulose. In contrast, the strain expressing neither cellulose nor curli (cellulose−/curli−) appeared pale in color (Figure 2A). Lastly, the presence of cellulose in the biofilm matrices was visualized by a calcofluor assay,[14] in which bacteria are grown on a supportive growth medium and calcofluor in the growth medium binds to bacterially produced cellulose to produce a fluorescent signal. The cellulose+/curli+ strains exhibited bright fluorescence under UV, indicating the presence of cellulose, while the strains not expressing cellulose (cellulose−/curli− or cellulose−/curli+) appeared nonfluorescent (Figure 2A) due to the absence of cellulose. Taken together, these results indicate that our bacterial strains expressing curli and/or cellulose were able to robustly produce biofilm matrix components upon

growth in liquid or hydrogel culture under our laboratory growth conditions.

We 3D-printed each of these three *E. coli* strains expressing cellulose and/or curli (cellulose+/curli+, cellulose−/curli+, cellulose−/curli−) biofilm matrix polymers as one-layered or four-layered stripes using our customized 3D bioprinter.[23,36] The 3D prints consisted of *E. coli* bacteria immobilized within a calcium alginate hydrogel. The alginate hydrogel serves as a cell-compatible physical support during the bacterial biofilm formation process. After 1 week of incubation at room temperature, the formed 3D-printed biofilms were tested for resistance to citrate treatment as a proxy to detect the formation of biofilm-matrix components (Figure 2B). Treatment with sodium citrate dissolves the alginate hydrogel matrix unless it is reinforced by biofilm-matrix polymers produced by the encapsulated bacteria.[37] Only the 3D prints expressing curli alone (cellulose−/curli+) or both curli and cellulose (cellulose+/curli+) were capable of resisting the citrate treatment, whereas the 3D prints containing no bacteria or bacteria expressing neither curli nor cellulose (cellulose−/curli−) were dissolved by citrate treatment. These results indicated that the *E. coli* strains expressing either curli alone or both curli and cellulose were capable of robust biofilm matrix production after 3D printing.

We examined the 3D printability of these *E. coli* biofilms by designing arbitrary shapes and patterns. A variety of different patterns of biofilms could be generated with this 3D printing approach (Figure 3). The production of cellulose in the 3D-printed biofilms was determined by visualizing the fluorescence of the 3D prints under UV by a calcofluor assay. 3D-printed biofilms expressing cellulose (cellulose+/curli+) showed bright fluorescence, whereas 3D-printed biofilms not expressing cellulose (cellulose−/curli+) or expressing no matrix components (cellulose−/curli−) appeared nonfluorescent (Figure 3, bottom). Thus, our approach makes it possible to 3D-print *E. coli* biofilms composed solely of curli or a combination of curli and cellulose while providing freedom of design and patterning.

3D-Printed *E. coli* Biofilms Display Limited Penetration of Molecular Oxygen. In natural biofilms, the spatial arrangement of cells within the biofilm has implications for their aerobic or anaerobic state. For instance, cells in the top layers of a biofilm are exposed to ambient levels of oxygen and therefore composed of fast-growing cells. In contrast, the intermediate and lower layers of the biofilm comprise an anaerobic zone of slow-
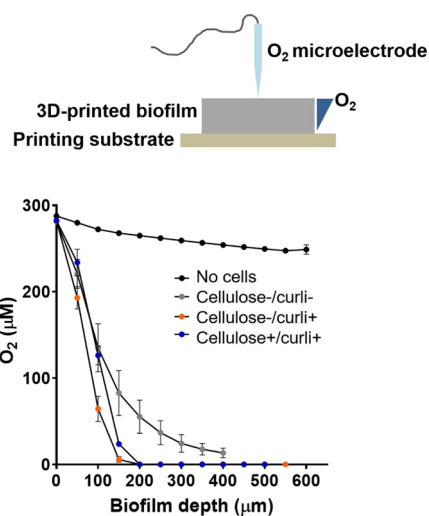
C
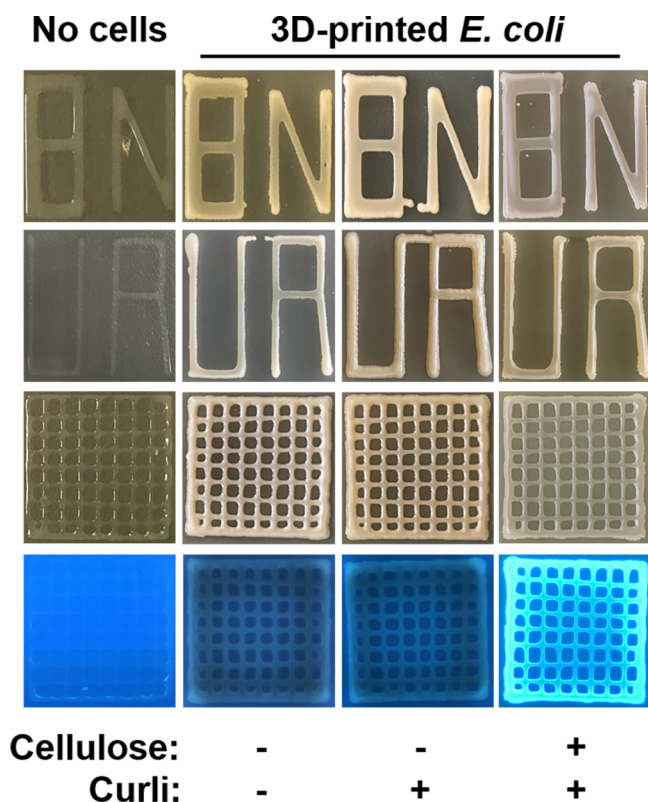
Figure 3. 3D printability of 7 day *E. coli* biofilms expressing cellulose and/or curli. Different types of possible patterning of 3D-printed biofilms (top three rows) and their fluorescence under UV in a calcofluor assay (bottom row). Calcofluor fluorescence under UV (wavelength: 312 nm) indicates cellulose production in the 3D-printed biofilms.

Figure 4. Oxygen profiles of four-layered 3D-printed biofilms revealing the presence of zero-O_2 zones in the bottom layers. An oxygen microelectrode was used to profile the oxygen concentration at different depths in 3D-printed *E. coli*. The deepest O_2 measurement coincides with the bottommost point of the 3D print at the interface with the supportive media such that the thickness of 3D prints can be compared with this method.

growing cells due to the limited diffusion of oxygen through the biofilm.[42,43] The altered growth and microbial metabolism of biofilm cells and the presence of slow-growing cells due to the anoxic zone has been hypothesized to lead to emergent resistance behavior of biofilms.[12,44,45] For instance, the oxygen-depleted state of *Pseudomonas aeruginosa* biofilms has been shown to contribute to increased antibiotic tolerance.[46]

In order to understand whether specific biofilm-matrix components were able to allow the 3D-printed biofilms to reproduce the anaerobic zones of native biofilms, we measured the oxygen penetration profile of 3D-printed biofilms with three different phenotypes (cellulose+/curli+, cellulose−/curli+ and cellulose−/curli−) at different depths using an oxygen micro-electrode system (Figure 4). The presence of oxygen within the 3D-printed *E. coli* varied noticeably in the presence of curli. Oxygen within the 3D-printed *E. coli* expressing cellulose+/curli+ and cellulose−/curli+ rapidly disappeared within the upper 200 μm of the biofilm, while oxygen reached the bottom (400 μm depth) of the 3D-printed *E. coli* expressing neither cellulose nor curli (cellulose−/curli−). *E. coli* 3D prints expressing cellulose+/curli+ and cellulose−/curli+ in their biofilms showed extended zero-oxygen zones of ∼300−400 μm in height. Hence, these 3D-printed curli+ biofilms presented anoxic conditions similar to native biofilms. This rapid decrease in oxygen concentration within the 3D prints expressing curli could be due to diffusion limitations rendered by increased density of the biofilm matrix (physical) as well as the microbial activity (biological).

In contrast, in the absence of biofilm extracellular-matrix components (cellulose−/curli−), microbial consumption of oxygen likely became the limiting factor for oxygen availability rather than physical diffusion of oxygen. No zero-oxygen zones were observed for the 3D-printed *E. coli* expressing neither curli nor cellulose (cellulose−/curli−). In the absence of cells and biofilm extracellular-matrix components (no cells), oxygen concentrations remained consistently high throughout the entire 3D-printed alginate hydrogel structure (thickness: 600 μm).

The thickness of the 3D prints studied using this method was determined. 3D-printed *E. coli* expressing cellulose and/or curli (cellulose+/curli+ and cellulose−/curli+) had a maximum thickness of 550 μm, whereas the 3D-printed *E. coli* expressing neither cellulose nor curli (cellulose−/curli−) had a maximum thickness of 400 μm. Hence, biofilms expressing the extracellular-matrix components cellulose and/or curli were thicker than the ones not expressing the extracellular-matrix components.

We compared the bacterial viability (cfu/mL) of the 3D prints per unit thickness among the 3D-printed biofilms expressing cellulose and/or curli (Figure S1). *E. coli* expressing cellulose and curli (cellulose+/curli+) demonstrated higher viability per unit thickness than *E. coli* expressing curli and no cellulose (cellulose−/curli+). Interestingly, *E. coli* expressing neither cellulose nor curli (cellulose−/curli−) exhibited higher viability per unit thickness than *E. coli* expressing curli and no cellulose (cellulose−/curli+). Thus, the production of curli may reduce the overall viability and/or density of the individual cells, and the lower oxygen concentrations in the cellulose−/curli+ strains cannot be attributed to an increased bacterial concentration in the biofilms as a whole. To fully understand the differences in oxygen profiles observed between different 3D-printed biofilms, further research is needed to determine the microscale distribution and activity of cells in the oxic layers of the 3D-printed biofilms, as well as the changes in the physical properties

of the biofilms due to curli and/or cellulose expression that may affect the diffusion of gases within the biofilms.

The reduction in oxygen concentration at lower biofilm depths for engineered 3D-printed curli+ biofilms could potentially have an impact on the viability or metabolic functioning of bacterial cells at these depths. Since the 3D-printed *E. coli* expressing curli only (cellulose−/curli+) also express GFP constitutively, we used confocal microscopy to assess whether GFP expression was observed at the lower depths of the biofilm (Figure S2). Confocal microscopy images indicated that cells at the lower depths of the biofilm expressed GFP robustly, whereas the GFP signal was not detected in the negative control cellulose+/curli+ 3D-printed biofilm lacking GFP production. These results indicated that even the deepest biofilm cells still showed viability in the 3D-printed cellulose−/curli+ biofilm, despite the low oxygen concentration.

Overall, we can conclude that 3D-printed biofilms that express either curli alone or both cellulose and curli closely resemble natural biofilm systems with respect to limited oxygen penetration through the biofilm matrix and the presence of a thicker anaerobic zone in the bottom layers of the biofilm.

Extracellular Matrix Composition Governs the Emergent Biological Endurance of 3D-Printed Biofilms. Bacteria in biofilms display biological endurance such as resistance to antimicrobials and disinfectants that their planktonic counterparts do not possess due to their marked 3D nature and the presence of the extracellular matrix that acts as a physical or chemical diffusion barrier.[11,47,48] While it is known that the molecular composition of the biofilm matrix has a major influence on the emergent *viscoelastic* mechanical properties of bacteria in biofilms,[13] the influence of the molecular composition of the biofilm matrix on the emergent *biological* properties remains unclear.

We aimed to solve this question by 3D printing different *E. coli* strains expressing curli only (cellulose−/curli+), both curli and cellulose (cellulose+/curli+), or neither curli nor cellulose (cellulose−/curli−) in their biofilm matrix and testing their biological endurance against exposure to varying concentrations of the widely used disinfectants ethanol and Virkon S (Figure 5). A schematic of the methodology for performing endurance assays is shown in Figure S3. The colony-forming units (cfus) of 3D-printed *E. coli* strains expressing neither cellulose nor curli (cellulose−/curli−), only curli (cellulose−/curli+), or both cellulose and curli (cellulose+/curli+) reached between 8 and 12 log(cfu/mL) after 7 days of incubation at room temperature (Figure 5). Treatment with ethanol at concentrations of 30−70% resulted in a dose-dependent reduction in the number of viable cells in each of the 3D-printed *E. coli* biofilms tested (Figure 5A). Since the bacterial strains each grew at different rates within the printed biofilms, we assessed resistance to antibacterial treatments by comparing log reductions in cfu/mL values. At the highest concentrations of 50 and 70% ethanol, 3D-printed *E. coli* expressing neither cellulose nor curli (cellulose−/curli−) was more sensitive to ethanol than the 3D-printed *E. coli* expressing cellulose and/or curli, leading to an approximate 5−6 log reduction in cfus/mL. 3D-printed *E. coli* expressing only curli (cellulose−/curli+) was more resistant to ethanol than the cellulose−/curli− strain, as shown by a smaller ~1.5−3 log reduction in cfu/mL upon treatment with 50−70% ethanol. In comparison to the cellulose−/curli+ strain, the 3D-printed *E. coli* expressing both cellulose and curli (cellulose+/curli+) revealed a lesser resistance to ethanol, with a ~3−5 log reduction in cfu/mL upon treatment with 50−70% ethanol.
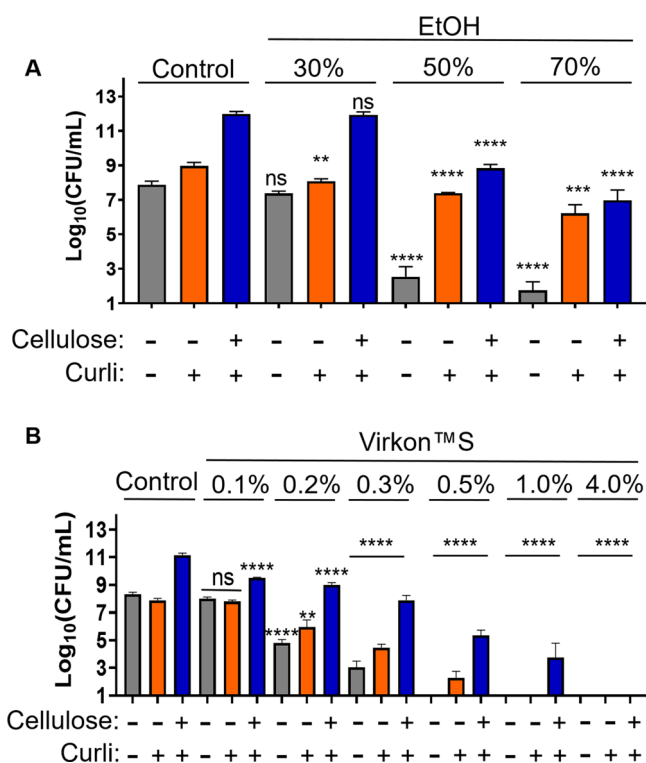
Figure 5. Emergent disinfectant resistance of 7 day-old 3D-printed biofilms to a 10 min exposure to varying concentrations of (A) ethanol or (B) Virkon S. Gray bars depict cellulose−/curli−, orange bars depict cellulose−/curli+, and blue bars depict cellulose+/curli+ 3D-printed *E. coli*. The control condition indicates treatment with sterile saline (0.9% (w/v) sodium chloride). Ns, not significant; **$p < 0.01$, ***$p < 0.001$, ****$p < 0.0001$. Statistical significance was assessed by comparing the disinfectant samples with their respective control sample using Student's *t*-test ($p < 0.05$; statistically significant).

Thus, the presence of curli fibers in the 3D-printed biofilms enhanced the resistance of *E. coli* to ethanol. The cellulose+/curli+ strain, which produced cellulose fibers in addition to the curli matrix, demonstrated a slightly reduced resistance to ethanol. These resistance phenotypes of the cellulose+/curli+ strain could potentially reflect inherent differences in biological resistance due to a different strain background as well as physical differences deriving from biofilm matrix composition; future experiments to tease apart the contributions to resistance from matrix polymers could resolve this question. In *E. coli* biofilms, curli fibers present in the biofilm extracellular matrix are known to dominate the biofilm mechanical behavior,[13,49] reflecting their strong internal structure and pronounced viscoelasticity. These properties provided by the curli fibers may be the cause of the emergent resistance to ethanol demonstrated by the resultant 3D-printed biofilms.

A similar trend of resistance to the disinfectant was observed upon the treatment of 7 day-old 3D-printed biofilms with Virkon S, a broad-spectrum disinfectant (Figure 5B). Exposure to increasing concentrations of Virkon S (0.1−4.0%) resulted in a dose-dependent reduction in the number of viable bacteria in each of the 3D-printed biofilms. The lowest concentration of Virkon S (0.1%) had little effect, leading to an approximate 1.6-log reduction in cfu/mL only in 3D-printed biofilms expressing both cellulose and curli (cellulose+/curli+), whereas the highest concentration of Virkon S tested (4.0%) resulted in 100% killing of bacteria in all of the 3D-printed biofilms. The protective

nature of curli and/or cellulose in conferring resistance was observable at Virkon S concentrations between 0.2 and 0.5%. At these concentrations, the reduction in cfus in comparison to untreated control samples was consistently 1−2 log lower for the 3D-printed biofilms expressing either only curli and no cellulose (cellulose−/curli+) or both cellulose and curli (cellulose+/curli +) in comparison to the reductions in cfus measured for the 3D-printed biofilms expressing neither cellulose nor curli (cellulose−/curli−). The biofilms expressing extracellular-matrix polymers were viable at higher concentrations of Virkon S; the highest concentration of Virkon S that allowed detectable viable cfus for each strain was 1.0% for cellulose+/curli+ biofilms and 0.5% for cellulose−/curli+ biofilms, in comparison to 0.3% for cellulose−/curli− biofilms. Moreover, at these concentrations the expression of both cellulose and curli (cellulose +/curli+) in the 3D-printed biofilm conferred a greater resistance to Virkon S than the expression of curli alone without cellulose (cellulose−/curli+).

We evaluated the sensitivity of 3D-printed biofilms to either ethanol [70% (v/v)] or Virkon S [0.5% (w/v)] at 2 days of growth, an early time point where biofilm-matrix components would be less expressed. The cfus of 3D-printed *E. coli* strains expressing neither cellulose nor curli (cellulose−/curli−), only curli and no cellulose (cellulose−/curli+), or both cellulose and curli (cellulose+/curli+) reached approximately 7−10 log cfu/mL after 2 days of incubation at room temperature (Figure 6). These values were approximately 10−100-fold lower than the values seen after 7 days of growth. Both the 3D-printed biofilms expressing neither cellulose nor curli (cellulose−/curli−) or only curli and no cellulose (cellulose−/curli+) showed complete sensitivity to either ethanol or Virkon S treatment, indicating the

absence of sufficient curli production to be protective at this time point. We have previously shown that curli production in these 3D-printed *E. coli* has occurred by 3 days of incubation at room temperature at levels sufficient to prevent citrate-based dissolving of the alginate matrix.[37] In contrast, 3D-printed biofilms expressing both cellulose and curli (cellulose+/curli+) showed marked resistance to both ethanol and Virkon S resulting in a survival of about 10^2−10^3 cfu/mL. This result indicates that cellulose production could happen much earlier in the 3D-printed biofilms than the curli production such that this resistance would be an emergent property resulting from cellulose in the matrix. Alternatively, the cellulose+/curli+ strain could produce more curli at earlier time points.

Thus, 3D prints of *E. coli* expressing biofilm matrix polymers (containing cellulose and/or curli) were more resistant to disinfectants than the 3D prints containing nonbiofilm-forming *E. coli* (neither cellulose nor curli). Based on our data, it is evident that the extracellular matrix composition, particularly the presence of curli fibers, plays an important role in development of biological endurance against disinfectants in 3D-printed *E. coli* biofilms. This result is in agreement with the results of previous studies that show that curli rather than cellulose expression is directly related to the emergent resistance of *E. coli* against sanitizers in 2D models.[16,50]

Effect of Tuning the Cell- and Matrix-Component Densities on Emergent Biofilm Endurance. In natural biofilms, the living (bacterial cells) and the nonliving components (extracellular-matrix components such as cellulose and curli) are spatially patterned, which has been hypothesized to give rise to their emergent behavior under extreme conditions.[12,15,51] However, the exact nature of such spatial patterns and the influence of changing the spatial patterns on the emergent behavior is not fully characterized. We investigated this topic by 3D printing monoculture or coculture inks containing different ratios of different biofilm-forming bacteria. First, we studied the influence of altering cell density using a step increase/decrease function (Figure 7A) on the emergent resistance to ethanol [70% (v/v)]. Bacteria expressing only curli and no cellulose (cellulose−/curli+) were 3D-printed as four-layered constructs with higher cell density in the bottom two layers and lower cell density in the top two layers or vice versa. In both configurations, the final cell density reached approximately ∼9 log cfu/mL after 7 days of incubation at room temperature. Treatment with ethanol resulted in ∼2 log reduction of cfu/mL in the configuration with higher cell density at the bottom and lower cell density at the top and ∼3.5 log reduction of cfu/mL in the configuration with lower cell density at the bottom and higher cell density at the top. Thus, the biofilm design with higher cell density at the bottom is more resistant to ethanol than the design with lower cell density at the bottom. This design with higher resistance also adopts the pattern of cell density distribution seen for most natural biofilms.[10]

Next, we studied whether tuning the curli density would lead to differences in the emergent resistance to ethanol. For this, we employed a step increase/decrease configuration of curli density during biofilm design, that is, we 3D-printed two layers of bioink containing *E. coli* expressing neither cellulose nor curli (cellulose−/curli−) overtop of two layers of 3D-printed bioink containing *E. coli* expressing only curli and no cellulose (cellulose−/curli+) or vice versa (Figure 7B). We also employed a gradient increase/decrease configuration of curli density, in which we 3D-printed the top two layers using coculture bioinks
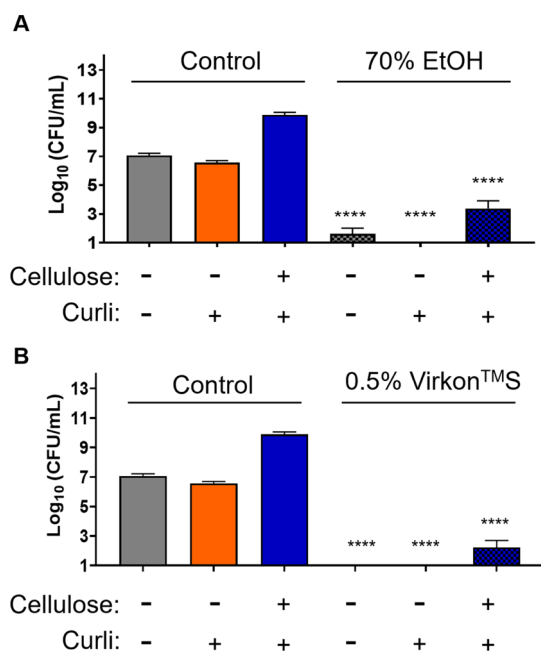
Figure 6. Sensitivity of 2 day-old 3D-printed biofilms to a 10 min exposure to (A) ethanol [70% (v/v)] or (B) Virkon S [0.5% (w/v)]. Gray bars depict cellulose−/curli−, orange bars depict cellulose−/curli +, and blue bars depict cellulose+/curli+ 3D-printed *E. coli*. The control condition indicates treatment with sterile saline [0.9% (w/v) sodium chloride]. ****$p < 0.0001$. Statistical significance between the ethanol or Virkon S samples versus the control samples was assessed with Student's *t*-test ($p < 0.05$; statistically significant).
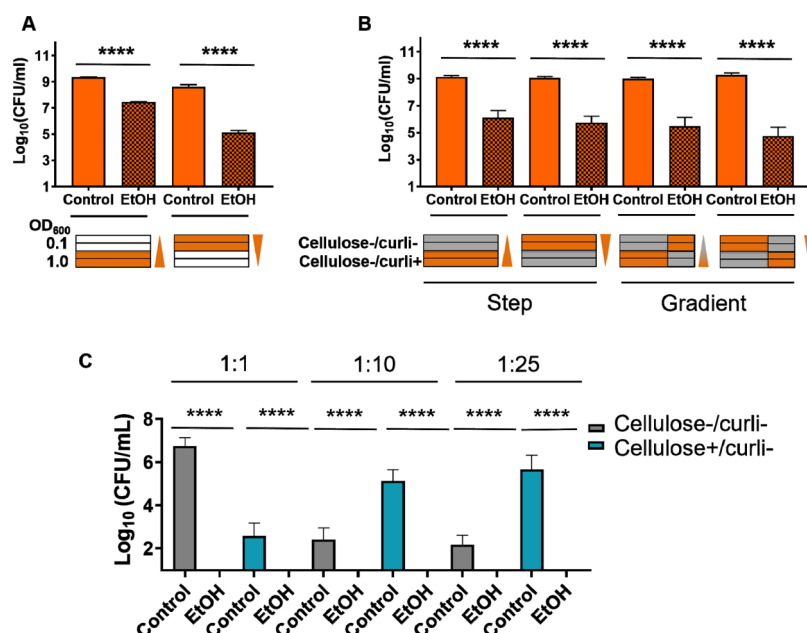
Figure 7. Effect of tuning the (A) bacterial density, (B) curli density, and (C) cellulose density on emergent endurance to ethanol [70% (v/v)]. (A) Bacterial density was varied by 3D printing cellulose−/curli+ bioinks as four-layered constructs with higher cell density (shown in orange color) in the bottom two layers and lower cell density (shown in white color) in the top two layers or vice versa. (B) Curli density was varied in a step function by 3D printing two layers of bioink containing *E. coli* expressing neither cellulose nor curli (cellulose−/curli−; shown in gray color) overtop of two layers of 3D-printed bioink containing *E. coli* expressing only curli and no cellulose (cellulose−/curli+; shown in orange color), or vice versa. Curli density was also varied in a gradient function by 3D printing two layers of coculture bioinks containing *E. coli* expressing neither cellulose nor curli (cellulose−/curli−) mixed with *E. coli* expressing only curli and no cellulose (cellulose−/curli+) in a ratio of 3:1 overtop of two layers of 3D-printed coculture bioinks containing *E. coli* expressing neither cellulose nor curli (cellulose−/curli−) mixed with *E. coli* expressing only curli and no cellulose [(cellulose−/curli+) in a ratio of 1:3] or vice versa. (C) Cellulose density was varied by 3D printing four-layered constructs of coculture bioinks containing *E. coli* expressing neither cellulose nor curli (cellulose−/curli−) mixed with *G. hansenii* (cellulose+/curli−) in ratios of 1:1, 1:10, or 1:25 (*E. coli/G. hansenii*). (A−C) The control conditions indicate treatment with sterile saline [0.9% (w/v) sodium chloride]. Ethanol treatment resulted in statistically significant reduction of bacterial cfus in each of the experiments, ****$p < 0.0001$. Statistical significance was assessed by comparing the disinfectant samples with their respective control samples using Student's *t*-test ($p < 0.05$; statistically significant).

containing *E. coli* expressing neither cellulose nor curli (cellulose−/curli−) mixed with *E. coli* expressing only curli and no cellulose (cellulose−/curli+) in a ratio of 3:1, overtop of two layers of 3D-printed coculture bioinks containing *E. coli* expressing neither cellulose nor curli (cellulose−/curli−) mixed with *E. coli* expressing only curli and no cellulose [(cellulose−/curli+) in a ratio of 1:3] or vice versa. In each configuration, the final cell density reached approximately ∼9 log cfu/mL after 7 days of incubation at room temperature. Treatment with ethanol resulted in ∼3 log reduction of cfu/mL in each of the four printed configurations. Thus, tuning the curli density by adjusting the proportion of curli-expressing bacteria in each layer during the 3D printing had no effect on the emergent resistance against ethanol.

Data from our earlier experiments indicated that cellulose production in 3D-printed biofilms could lead to emergence of resistance to ethanol and Virkon S (Figure 6). In order to further understand this phenomenon, we evaluated whether tuning the cellulose density could lead to differences in the emergent resistance to ethanol. To achieve this, we employed 3D printing of coculture bioinks containing *E. coli* expressing neither cellulose nor curli (cellulose−/curli−) mixed with *Gluconacetobacter hansenii*, a bacterium that produces copious cellulose but not curli fibers.[52] The two strains were mixed in ratios of 1:1, 1:10, or 1:25 and printed to make four-layered constructs. To study their emergent resistance to ethanol, the individual survival rates of *E. coli* and *G. hansenii* were determined by plating the samples onto Luria−Bertani (LB) agar supple-

mented with chloramphenicol (selective for *E. coli*) or HS agar supplemented with acetic acid (selective for *G. hansenii*). Determination of cfu values revealed that both the *E. coli* and *G. hansenii* strains were able to grow in the 3D-printed coculture inks (Figure 7C). As the ratio of *E. coli* to *G. hansenii* increased from 1:1 to 1:25 in the bioinks, the cfus of *G. hansenii* in the fully grown mock-treated 3D prints increased from ∼3 to 6 log cfu/mL, and the cfus of *E. coli* decreased from ∼6 to 2 log cfu/mL. Following ethanol treatment, a survival rate of 0 cfus/mL was measured for both *E. coli* and *G. hansenii* in each 3D-printed biofilm, indicating that none of the 3D-printed biofilms displayed emergent resistance to ethanol for either species. Thus, cellulose alone in the biofilm matrix cannot confer emergent endurance against ethanol to 3D-printed biofilms in our tested conditions. *G. hansenii* has been shown to produce higher-ordered crystalline cellulose, whereas *E. coli* produces lesser-ordered amorphous forms of cellulose.[52] SEM images of our *G. hansenii* and *E. coli* Nissle (cellulose+/curli+) colony biofilms also revealed differences in the biofilm architecture of the two strains (Figure S4). Hence, differences in the network and the microstructure properties of *G. hansenii* cellulose in comparison with the *E. coli* cellulose could contribute to the absence of protection to *E. coli* against ethanol in our experiments. In the future, a better understanding into this phenomenon could be obtained using a strain of *E. coli* that produces high amounts of cellulose but not curli.

Physical Stability of 3D-Printed Biofilms. 3D-printed biofilms could be used in various beneficial applications
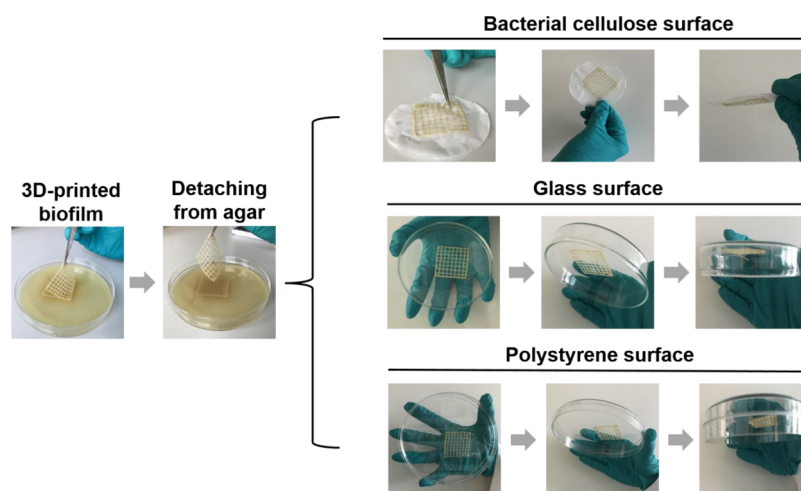
Figure 8. Adhesion of 3D-printed *E. coli* cellulose+/curli+ biofilms to bacterial cellulose, glass, and polystyrene surfaces after detachment from agar.

Table 1. Strains Used in This Study

strains used in this study	phenotype	reference and/or source
E. coli MG1655 PRO Δ*csgA ompR234* (*E. coli* Δ*csgA*) carrying plasmid pSB1C3-GFP (constitutive GFP expression)	cellulose−/curli−	36, 37
E. coli MG1655 PRO Δ*csgA ompR234* (*E. coli* Δ*csgA*) carrying plasmid AM404 (constitutive GFP and rhamnose-inducible CsgA)	cellulose−/curli+	36, 37
E. coli Nissle (wildtype)	cellulose+/curli+	University of Wuerzburg[53]
Gluconacetobacter hansenii ATCC 53582	cellulose+/curli−	American Type Culture Collection (ATCC)

including bioremediation, wastewater treatment, or probiotic coatings on medical devices and surfaces to prevent colonization by pathogenic bacteria. In order to be employed in such applications, reversible adhesion of 3D-printed biofilms to different surfaces and physical stability are important aspects. We tested these parameters by removing fully grown (7 days old) 3D-printed *E. coli* (cellulose+/curli+) biofilms from agar and attaching them to fresh surfaces composed of bacterial cellulose, glass, or polystyrene (Video S1). The 3D-printed biofilms displayed reversible attachment to fresh bacterial cellulose as well as glass and polystyrene surfaces (Figure 8).

Since our 3D-printed biofilms adhered to bacterial cellulose, which is sustainably produced and possesses excellent mechanical properties including remarkable tensile strength (73−194 MPa) and toughness (2−25 MJ m⁻³),[19,31] we studied the deformation of the 3D-printed biofilms. Bacterial cellulose has been found to be a flexible substrate to support hydrogel-based living materials.[31] We further subjected the 3D-printed biofilms on the bacterial cellulose surface to manual distortions by folding, twisting, and crushing them (Figure S5). The 3D-printed biofilms resumed their original shapes upon unfolding, untwisting, and uncrushing, indicating their high physical stability. Thus, 3D-printed biofilms may be used as physically resilient materials for desired applications merely by attaching them to mechanically robust surfaces such as bacterial cellulose.

CONCLUSIONS

Taken together, our findings indicate that 3D printing can be effectively employed for studying the emergent biological endurance of bacterial biofilms by tuning the design principles and bioink composition (using monoculture or coculture inks). 3D-printed biofilms closely mimic natural biofilms in terms of their spatial heterogeneity and diffusion of molecular oxygen. Oxygen penetration in 3D-printed biofilms (expressing cellulose

and/or curli) is limited such that the top layers are exposed to oxygen, whereas the layers toward the bottom exhibit an anaerobic state. The composition of the extracellular matrix is crucial for determining the resultant emergence of resistance against disinfectants. 3D-printed biofilms expressing either only curli or both curli and cellulose are more resistant to ethanol and Virkon S than the 3D prints expressing cellulose alone, indicating the protective nature of curli fibers. 3D-printed biofilms retain an adhesive nature and can be reversibly attached to different surfaces such as bacterial cellulose, glass, and polystyrene. The physical stability of 3D-printed biofilms on mechanically robust bacterial cellulose surfaces and their biological endurance to extreme environmental conditions highlights their suitability for such applications as protective probiotic coatings on medical devices that prevent colonization by pathogens, degradation of toxic chemicals, bioremediation, or use in wastewater treatment facilities, among many others.

METHODS

Reagents, Bacterial Strains, and Propagation. The chemical reagents and solvents used in this study [agar, anhydrous disodium phosphate, calcium chloride, calcofluor (fluorescent brightener), cellulase from *Trichoderma reesei* (aqueous solution, ≥700 units g⁻¹), chloramphenicol, citric acid, Congo red, crystal violet, ethanol, glucose, rhamnose, sodium alginate, sodium chloride, sodium citrate, tryptone, and yeast extract] were purchased from Sigma-Aldrich. Virkon S was purchased from Biosecurity B.V.

The bacterial strains used in this study are listed in Table 1.

Overnight cultures of *E. coli* Nissle wildtype strain were grown in LB medium (sodium chloride: 10.0 g L⁻¹, yeast extract: 5.0 g L⁻¹, tryptone: 10 g L⁻¹) under continuous shaking at 200 rpm at 37 °C overnight. Experiments with *E. coli* Nissle wildtype were subsequently carried out on LB agar plates. *E. coli* MG1655

strains carrying plasmids were cultured in LB medium supplemented with 34 μg mL^{-1} chloramphenicol under continuous shaking at 200 rpm at 37 °C overnight. Chemical induction of *csgA* was performed using an inducer concentration of 0.5% (w/v) rhamnose. Experiments with these strains were subsequently carried out on LB agar plates supplemented with either 34 μg mL^{-1} chloramphenicol (cellulose−/curli−) or 34 μg mL^{-1} chloramphenicol with 0.5% (w/v) rhamnose (cellulose−/curli+).

G. hansenii was cultured in Hestrin−Schramm (HS) medium (tryptone: 5.0 g L^{-1}, yeast extract: 5.0 g L^{-1}, disodium hydrogen phosphate: 2.7 g L^{-1}, citric acid: 1.5 g L^{-1}, and glucose: 20 g L^{-1}) statically at 30 °C for 7 days to obtain a bacterial cellulose pellicle at the air−liquid interface.[31] Overnight cultures of *G. hansenii* were then prepared by dissolving the cellulose pellicle with cellulase (0.1 v/v %) by shaking at 180 rpm at 30 °C overnight. The obtained solution was then centrifuged at 4000 rpm for 5 min at 4 °C to obtain the cells for further experiments. Experiments with *G. hansenii* were subsequently carried out on HS agar plates with incubation at 30 °C for 7 days.

Biofilm Formation in Glass Tubes. The biofilm formation of *E. coli* strains under investigation was characterized by a crystal violet assay. In brief, bacterial strains (O.D.$_{600}$ of 0.1) in LB medium [or LB medium supplemented with chloramphenicol (34 μg mL^{-1})] and/or rhamnose [0.5% (w/v)] were incubated in glass test tubes (15 × 2.2 cm) at room temperature for 7 days. Planktonic cells were discarded, and the tubes were washed twice with sterile water. Biofilm cells at the air−liquid interface were stained with 10 mL of crystal violet [0.1% (w/v)] for 5 min. The samples were further washed with sterile water 3 times to remove the unbound crystal violet and air-dried at room temperature. The tubes were then photographed to visualize the crystal violet-stained biofilms. Experiments were repeated at least twice.

Detection of Cellulose and/or Curli. The production of curli and/or cellulose by *E. coli* strains in the study was assessed by Congo red and calcofluor assay as previously described[14] following minor modifications. In brief, 10 μL of overnight culture of the *E. coli* strains was spotted onto the appropriate agar plates (LB, LB + chloramphenicol, or LB + chloramphenicol + rhamnose) supplemented with Congo red (50 μg mL^{-1}) or calcofluor (200 μg mL^{-1}). Plates were incubated at room temperature for 7 days. After incubation, Congo red plates were photographed to assess curli and/or cellulose production. Bacteria on calcofluor plates were imaged on a UV trans-illuminator (Syngene, wavelength: 312 nm) to assess fluorescence due to cellulose production.

Bioink Preparation. Bioinks for 3D printing were prepared by combining a specific strain of *E. coli* (grown overnight at 37 °C and diluted in fresh LB medium to an O.D.$_{600}$ of 0.2) with an equal volume of sterile sodium alginate [5% (w/v)]. Coculture inks for 3D printing were prepared by mixing different ratios of two different strains of *E. coli* or *E. coli* with *G. hansenii*, together with an equal volume of sodium alginate [5% (w/v)].

Printing Substrate Preparation. 3D printing of bacterial bioinks containing *E. coli* was performed on LB agar plates [1.5% (w/v)] supplemented with appropriate antibiotics and/or inducers, and 3D printing of bacterial bioinks containing *G. hansenii* with or without *E. coli* was performed on HS agar plates. Coculture bioinks containing both an *E. coli* MG1655 strain and *G. hansenii* were printed onto HS agar without antibiotics. To permit the alginate hydrogel formation during the printing

procedure, all the plates were additionally supplemented with 0.05 M CaCl$_2$ before agar solidification.

3D Printing. 3D printing of bacteria was carried out with a do-it-yourself 3D printer that has been previously shown to effectively 3D print *E. coli* in spatially defined patterns.[23,36] 3D structures with desired shapes and patterns were printed with this printer by manually programming the G-codes in the CoLiDo printing software. An extrusion rate of 0.3 ml h^{-1} was maintained throughout the printing process to ensure high printing resolution.

Citrate Treatment. Petri dishes containing 7 day-old one- or four-layered 3D-printed *E. coli* printed overtop of LB agar were filled with 25 mL of sodium citrate (0.5 M) and shaken at 40 rpm for 2 h at ambient temperature. The samples were imaged before and after the citrate treatment to visualize the dissolution of the alginate hydrogel.

Oxygen Profiling. 3D prints were vertically profiled using an oxygen microelectrode (Unisense A.S, Arhus, Denmark) at 50−100 μm resolution (tip size: 50 μm) at room temperature (18 °C). During microsensor profiling, a stream of air from an air pump was provided over the surface of the biofilm (or agar) to ensure a well-mixed layer at the air−biofilm interface. A two-point calibration was made with 100% air saturation above the biofilm (160−130 mV) and 0% air saturation at the anoxic layer of the biofilm (<5 mV). Oxygen depth profiles were recorded in 50 μm stepwise increments with a 2 s waiting time between measurements and 2 s duration for each measurement. Oxygen measurements were started at least 500 μm (>10 measurements) above the biofilm (in air) and finalized once oxygen concentrations dropped below 1 μM. After each profile, the microelectrode was rinsed with Milli-Q to remove any residual material on the tip.

Confocal Microscopy. Confocal microscopy 3D images of 1 week-old 3D-printed *E. coli* biofilms (four-layered) expressing curli and with constitutive GFP expression (cellulose−/curli+) or *E. coli* expressing both curli and cellulose (cellulose+/curli+) but no GFP expression were acquired with a Nikon A1R confocal inverted microscope equipped with a Nikon Plan Apo 20×/0.75 NA dry objective lens and optimized for GFP fluorescence detection (488 nm excitation laser line and 525/25 nm emission filter). The image acquisition was performed using Nikon NIS element software, and the following parameters were kept constant for all the 3D images: pixel size of 410 nm; voxel size of 2 μm; 488 nm laser power set to 0.8%; GaAsP detector gain set to 25. A depth of 108 μm was acquired from the bottom of the biofilm for *E. coli* expressing curli only (cellulose−/curli+), and 74 μm was acquired for *E. coli* expressing both cellulose and curli (cellulose+/curli+). Images were processed with Fiji software.

Testing the Effect of Disinfectants on 3D-Printed Biofilms. 3D-printed biofilms (four-layered lines) together with their agar substrates were cut into square pieces (10 × 10 mm) and transferred to six-well plates. The samples were immersed in 4 mL of sterile saline [0.9 NaCl % (w/v)] or varying concentrations of EtOH [0, 30, 50, and 70% (v/v)] or Virkon S [0.1, 0.2, 0.3, 0.5, 1.0, and 4.0% (w/v)] for 10 min. After exposure, the 3D prints were immersed in 1 mL of sodium citrate (0.5 M) for 10 min with continuous vortexing to dissolve the alginate hydrogel and recover the bacteria. Serial dilutions (10^0−10^8) of these samples were then made in saline, and 10 μL was spotted onto the respective selective media plates (LB agar for Nissle wildtype, LB agar with chloramphenicol for MG1655 strains carrying plasmids, or HS agar with acetic acid for *G.*

hansenii). Plates with bacteria were incubated at 37 °C overnight (*E. coli* strains) or 30 °C for 6 days (*G. hansenii*). The cfus were enumerated, and log(cfu/mL) values were calculated to assess the effectiveness of disinfectants on 3D-printed biofilms.

Scanning Electron Microscopy. Biofilms of *G. hansenii* (on HS agar) and *E. coli* Nissle (cellulose+/curli+) (on LB agar) were grown as colonies at 30 °C for 7 days. Biofilms were then fixed with glutaraldehyde (6.25 w/v %) in Sorenson's phosphate buffer overnight at 4 °C, dehydrated with increasing gradients of ethanol (30, 50, 70, and 100 v/v %), and air-dried. The samples were sputter-coated with gold−palladium at 20 mA for 60 s and observed at 5−15 kV under vacuum in SEI mode with a scanning electron microscope (JEOL JSM 6010 LA).

Stability Assessments of 3D-Printed Biofilms on Different Materials. A week-old *E. coli* biofilm was detached from the agar surface using tweezers and deposited onto alternate fresh surfaces such as bacterial cellulose (prepared as described previously[31]), glass, or polystyrene plates. The samples were then inverted to assess the adhesion of the 3D-printed biofilms to the new surfaces and photographed. The stability to physical distortion of 3D-printed biofilms on bacterial cellulose was investigated by manually crushing, folding, or twisting the sample. The samples were subsequently unfolded, untwisted, or uncrushed and photographed.

Statistical Analysis. Each experiment was performed in two independent trials with at least four technical replicates each time ($n = 8$ in total). Statistical comparisons between different controls and treatments were performed with Student's *t*-test using GraphPad Prism software (version 9.1.2).

◼ ASSOCIATED CONTENT

Ⓢ Supporting Information

The Supporting Information is available free of charge at https://pubs.acs.org/doi/10.1021/acssynbio.1c00290.

> Bacterial viability per unit thickness, GFP expression at lower biofilm depths, schematic representation of biofilm resistance assays, SEM biofilm images, manual distortion of 3D-printed biofilms on bacterial cellulose (PDF)

> Detaching and reattaching a 3D-printed *E. coli* cellulose +/curli+ biofilm sequentially to bacterial cellulose, glass, and polystyrene surfaces after detachment from agar (MOV)

◼ AUTHOR INFORMATION

Corresponding Authors

Marie-Eve Aubin-Tam − *Department of Bionanoscience & Kavli Institute of Nanoscience, Delft University of Technology, 2629 HZ Delft, The Netherlands;* ⓞ orcid.org/0000-0001-9995-2623; Phone: +31 (0)15 27 82853; Email: M.E.Aubin-Tam@tudelft.nl

Anne S. Meyer − *Department of Biology, University of Rochester, Rochester, New York 14627, United States;* ⓞ orcid.org/0000-0002-4164-0122; Phone: 1(585)-275-9290; Email: anne.meyer@rochester.edu

Authors

Srikkanth Balasubramanian − *Department of Sustainable Design Engineering, Faculty of Industrial Design Engineering, Delft University of Technology, 2628 CE Delft, The Netherlands*

Kui Yu − *Department of Bionanoscience & Kavli Institute of Nanoscience, Delft University of Technology, 2629 HZ Delft, The Netherlands*

Diana Vasquez Cardenas − *Department of Biotechnology, Delft University of Technology, 2629 HZ Delft, The Netherlands*

Complete contact information is available at:
https://pubs.acs.org/10.1021/acssynbio.1c00290

Author Contributions

S.B., M.-E.A.-T., and A.S.M. designed the experiments. S.B., K.Y., and D.V.C. conducted the experiments and analyzed the data. All authors subsequently wrote and modified the manuscript jointly. The final manuscript was approved by all the authors.

Notes

The authors declare no competing financial interest.

◼ REFERENCES

(1) Flemming, H.-C.; Wingender, J. The biofilm matrix. *Nat. Rev. Microbiol.* **2010**, *8*, 623−633.

(2) Flemming, H.-C.; Wingender, J.; Szewzyk, U.; Steinberg, P.; Rice, S. A.; Kjelleberg, S. Biofilms: an emergent form of bacterial life. *Nat. Rev. Microbiol.* **2016**, *14*, 563−575.

(3) Bjarnsholt, T. The role of bacterial biofilms in chronic infections. *APMIS* **2013**, *121*, 1−58.

(4) Chen, A. Y.; Deng, Z.; Billings, A. N.; Seker, U. O. S.; Lu, M. Y.; Citorik, R. J.; Zakeri, B.; Lu, T. K. Synthesis and patterning of tunable multiscale materials with engineered cells. *Nat. Mater.* **2014**, *13*, 515−523.

(5) Hufnagel, D. A.; Depas, W. H.; Chapman, M. R. The Biology of the Escherichia coli Extracellular Matrix. *Microbiol. Spectrum* **2015**, *3*, 3.3.23.

(6) Ntsama-Essomba, C.; Bouttier, S.; Ramaldes, M.; Dubois-Brissonnet, F.; Fourniat, J. Resistance of Escherichia coli growing as biofilms to disinfectants. *Vet. Res.* **1997**, *28*, 353−363.

(7) Bjarnsholt, T.; Buhlin, K.; Dufrêne, Y. F.; Gomelsky, M.; Moroni, A.; Ramstedt, M.; Rumbaugh, K. P.; Schulte, T.; Sun, L.; Åkerlund, B.; Römling, U. Biofilm formation - what we can learn from recent developments. *J. Intern. Med.* **2018**, *284*, 332−345.

(8) Ito, A.; Taniuchi, A.; May, T.; Kawata, K.; Okabe, S. Increased antibiotic resistance of Escherichia coli in mature biofilms. *Appl. Environ. Microbiol.* **2009**, *75*, 4093−4100.

(9) Hall-Stoodley, L.; Costerton, J. W.; Stoodley, P. Bacterial biofilms: from the natural environment to infectious diseases. *Nat. Rev. Microbiol.* **2004**, *2*, 95−108.

(10) Balasubramanian, S.; Aubin-Tam, M.-E.; Meyer, A. S. 3D Printing for the Fabrication of Biofilm-Based Functional Living Materials. *ACS Synth. Biol.* **2019**, *8*, 1564−1567.

(11) Amanatidou, E.; Matthews, A. C.; Kuhlicke, U.; Neu, T. R.; McEvoy, J. P.; Raymond, B. Biofilms facilitate cheating and social exploitation of beta-lactam resistance in Escherichia coli. *npj Biofilms Microbiomes* **2019**, *5*, 36.

(12) Grobas, I.; Bazzoli, D. G.; Asally, M. Biofilm and swarming emergent behaviours controlled through the aid of biophysical understanding and tools. *Biochem. Soc. Trans.* **2020**, *48*, 2903−2913.

(13) Horvat, M.; Pannuri, A.; Romeo, T.; Dogsa, I.; Stopar, D. Viscoelastic response of Escherichia coli biofilms to genetically altered expression of extracellular matrix components. *Soft Matter* **2019**, *15*, 5042−5051.

(14) Serra, D. O.; Richter, A. M.; Hengge, R. Cellulose as an Architectural Element in Spatially Structured Escherichia coli Biofilms. *J. Bacteriol.* **2013**, *195*, 5540.

(15) Nadezhdin, E.; Murphy, N.; Dalchau, N.; Phillips, A.; Locke, J. C. W. Stochastic pulsing of gene expression enables the generation of spatial patterns in Bacillus subtilis biofilms. *Nat. Commun.* **2020**, *11*, 950.

(16) Wang, R.; Bono, J. L.; Kalchayanand, N.; Shackelford, S.; Harhay, D. M. Biofilm formation by Shiga toxin-producing Escherichia coli O157:H7 and Non-O157 strains and their tolerance to sanitizers commonly used in the food processing environment. *J. Food Prot.* **2012**, *75*, 1418−1428.

(17) Gona, R. S.; Meyer, A. S. Engineered proteins and three-dimensional printing of living materials. *MRS Bull.* **2020**, *45*, 1034−1038.

(18) Banerjee, D.; Shivapriya, P. M.; Gautam, P. K.; Misra, K.; Sahoo, A. K.; Samanta, S. K. A Review on Basic Biology of Bacterial Biofilm Infections and Their Treatments by Nanotechnology-Based Approaches. *Proc. Natl. Acad. Sci., India, Sect. B* **2020**, *90*, 243−259.

(19) Nguyen, P. Q.; Courchesne, N. D.; Duraj-Thatte, A.; Praveschotinunt, P.; Joshi, N. S. Engineered Living Materials: Prospects and Challenges for Using Biological Systems to Direct the Assembly of Smart Materials. *Adv. Mater.* **2018**, *30*, 1704847.

(20) Srubar, W. V., 3rd. Engineered Living Materials: Taxonomies and Emerging Trends. *Trends Biotechnol.* **2021**, *39*, 574−583.

(21) Arrabito, G.; Ferrara, V.; Bonasera, A.; Pignataro, B. Artificial Biosystems by Printing Biology. *Small* **2020**, *16*, 1907691.

(22) Johnston, T. G.; Fillman, J. P.; Priks, H.; Butelmann, T.; Tamm, T.; Kumar, R.; Lahtvee, P. J.; Nelson, A. Cell-Laden Hydrogels for Multikingdom 3D Printing. *Macromol. Biosci.* **2020**, *20*, 2000121.

(23) Lehner, B. A. E.; Schmieden, D. T.; Meyer, A. S. A Straightforward Approach for 3D Bacterial Printing. *ACS Synth. Biol.* **2017**, *6*, 1124−1130.

(24) Seidel, J.; Ahlfeld, T.; Adolph, M.; Kümmritz, S.; Steingroewer, J.; Krujatz, F.; Bley, T.; Gelinsky, M.; Lode, A. Green bioprinting: extrusion-based fabrication of plant cell-laden biopolymer hydrogel scaffolds. *Biofabrication* **2017**, *9*, 045011.

(25) Gu, Y.; Schwarz, B.; Forget, A.; Barbero, A.; Martin, I.; Shastri, V. P. Advanced Bioink for 3D Bioprinting of Complex Free-Standing Structures with High Stiffness. *Bioengineering* **2020**, *7*, 141.

(26) Bhardwaj, A.; Vasselli, J.; Lucht, M.; Pei, Z.; Shaw, B.; Grasley, Z.; Wei, X.; Zou, N. 3D Printing of Biomass-Fungi Composite Material: A Preliminary Study. *Manuf. Lett.* **2020**, *24*, 96−99.

(27) Huang, J.; Liu, S.; Zhang, C.; Wang, X.; Pu, J.; Ba, F.; Xue, S.; Ye, H.; Zhao, T.; Li, K.; Wang, Y.; Zhang, J.; Wang, L.; Fan, C.; Lu, T. K.; Zhong, C. Programmable and printable Bacillus subtilis biofilms as engineered living materials. *Nat. Chem. Biol.* **2019**, *15*, 34−41.

(28) Qian, F.; Zhu, C.; Knipe, J. M.; Ruelas, S.; Stolaroff, J. K.; DeOtte, J. R.; Duoss, E. B.; Spadaccini, C. M.; Henard, C. A.; Guarnieri, M. T.; Baker, S. E. Direct Writing of Tunable Living Inks for Bioprocess Intensification. *Nano Lett.* **2019**, *19*, 5829−5835.

(29) González, L. M.; Mukhitov, N.; Voigt, C. A. Resilient living materials built by printing bacterial spores. *Nat. Chem. Biol.* **2020**, *16*, 126−133.

(30) Gilbert, C.; Ellis, T. Biological Engineered Living Materials: Growing Functional Materials with Genetically Programmable Properties. *ACS Synth. Biol.* **2019**, *8*, 1−15.

(31) Balasubramanian, S.; Yu, K.; Meyer, A. S.; Karana, E.; Aubin-Tam, M.-E. Bioprinting of Regenerative Photosynthetic Living Materials. *Adv. Funct. Mater.* **2021**, *31*, 2011162.

(32) Liu, X.; Yuk, H.; Lin, S.; Parada, G. A.; Tang, T. C.; Tham, E.; de la Fuente-Nunez, C.; Lu, T. K.; Zhao, X. 3D Printing of Living Responsive Materials and Devices. *Adv. Mater.* **2018**, *30*, 1704821.

(33) Schaffner, M.; Rühs, P. A.; Coulter, F.; Kilcher, S.; Studart, A. R. 3D printing of bacteria into functional complex materials. *Sci. Adv.* **2017**, *3*, No. eaao6804.

(34) Kyle, S. 3D Printing of Bacteria: The Next Frontier in Biofabrication. *Trends Biotechnol.* **2018**, *36*, 340−341.

(35) Ning, E.; Turnbull, G.; Clarke, J.; Picard, F.; Riches, P.; Vendrell, M.; Graham, D.; Wark, A. W.; Faulds, K.; Shu, W. 3D bioprinting of mature bacterial biofilms for antimicrobial resistance drug testing. *Biofabrication* **2019**, *11*, 045018.

(36) Spiesz, E. M.; Yu, K.; Lehner, B. A. E.; Schmieden, D. T.; Aubin-Tam, M. E.; Meyer, A. S. Three-dimensional Patterning of Engineered Biofilms with a Do-it-yourself Bioprinter. *J. Visualized Exp.* **2019**, *147*, No. e59477.

(37) Schmieden, D. T.; Basalo Vázquez, S. J.; Sangüesa, H.; van der Does, M.; Idema, T.; Meyer, A. S. Printing of Patterned, Engineered E. coli Biofilms with a Low-Cost 3D Printer. *ACS Synth. Biol.* **2018**, *7*, 1328−1337.

(38) Krasteva, P. V.; Bernal-Bayard, J.; Travier, L.; Martin, F. A.; Kaminski, P.-A.; Karimova, G.; Fronzes, R.; Ghigo, J.-M. Insights into the structure and assembly of a bacterial cellulose secretion system. *Nat. Commun.* **2017**, *8*, 2065.

(39) Thongsomboon, W.; Werby, S. H.; Cegelski, L. Evaluation of Phosphoethanolamine Cellulose Production among Bacterial Communities Using Congo Red Fluorescence. *J. Bacteriol.* **2020**, *202*, No. e00030.

(40) Hobley, L.; Harkins, C.; MacPhee, C. E.; Stanley-Wall, N. R. Giving structure to the biofilm matrix: an overview of individual strategies and emerging common themes. *FEMS Microbiol. Rev.* **2015**, *39*, 649−669.

(41) Kan, A.; Birnbaum, D. P.; Praveschotinunt, P.; Joshi, N. S. Congo Red Fluorescence for Rapid In Situ Characterization of Synthetic Curli Systems. *Appl. Environ. Microbiol.* **2019**, *85*, No. e00434.

(42) Walters, M. C., 3rd; Roe, F.; Bugnicourt, A.; Franklin, M. J.; Stewart, P. S. Contributions of antibiotic penetration, oxygen limitation, and low metabolic activity to tolerance of Pseudomonas aeruginosa biofilms to ciprofloxacin and tobramycin. *Antimicrob. Agents Chemother.* **2003**, *47*, 317−323.

(43) Cunningham, A. B.; Lennox, J. E.; Ross, R. J. *Biofilm: The Hypertextbook*; Montana State university: USA, 2011.

(44) Kim, W.; Racimo, F.; Schluter, J.; Levy, S. B.; Foster, K. R. Importance of positioning for microbial evolution. *Proc. Natl. Acad. Sci. U.S.A.* **2014**, *111*, E1639−E1647.

(45) Wu, Y.; Klapper, I.; Stewart, P. S. Hypoxia arising from concerted oxygen consumption by neutrophils and microorganisms in biofilms. *Pathog. Dis.* **2018**, *76*, fty043.

(46) Borriello, G.; Werner, E.; Roe, F.; Kim, A. M.; Ehrlich, G. D.; Stewart, P. S. Oxygen limitation contributes to antibiotic tolerance of Pseudomonas aeruginosa in biofilms. *Antimicrob. Agents Chemother.* **2004**, *48*, 2659−2664.

(47) Olsen, I. Biofilm-specific antibiotic tolerance and resistance. *Eur. J. Clin. Microbiol. Infect. Dis.* **2015**, *34*, 877−886.

(48) Bridier, A.; Briandet, R.; Thomas, V.; Dubois-Brissonnet, F. Resistance of bacterial biofilms to disinfectants: a review. *Biofouling* **2011**, *27*, 1017−1032.

(49) Collinson, S. K.; Emödy, L.; Müller, K. H.; Trust, T. J.; Kay, W. W. Purification and characterization of thin, aggregative fimbriae from Salmonella enteritidis. *J. Bacteriol.* **1991**, *173*, 4773−4781.

(50) Vogeleer, P.; Tremblay, Y. D. N.; Jubelin, G.; Jacques, M.; Harel, J. Biofilm-Forming Abilities of Shiga Toxin-Producing Escherichia coli

Isolates Associated with Human Infections. *Appl. Environ. Microbiol.* **2015**, *82*, 1448−1458.

(51) Kim, D.; Barraza, J. P.; Arthur, R. A.; Hara, A.; Lewis, K.; Liu, Y.; Scisci, E. L.; Hajishengallis, E.; Whiteley, M.; Koo, H. Spatial mapping of polymicrobial communities reveals a precise biogeography associated with human dental caries. *Proc. Natl. Acad. Sci. U.S.A.* **2020**, *117*, 12375−12386.

(52) Nicolas, W. J.; Ghosal, D.; Tocheva, E. I.; Meyerowitz, E. M.; Jensen, G. J. Structure of the Bacterial Cellulose Ribbon and Its Assembly-Guiding Cytoskeleton by Electron Cryotomography. *J. Bacteriol.* **2021**, *203*, No. e00371.

(53) Reister, M.; Hoffmeier, K.; Krezdorn, N.; Rotter, B.; Liang, C.; Rund, S.; Dandekar, T.; Sonnenborn, U.; Oelschlaeger, T. A. Complete genome sequence of the gram-negative probiotic Escherichia coli strain Nissle 1917. *J. Biotechnol.* **2014**, *187*, 106−107.

L